IMMUNOLOGY

Microbiota-dependent activation of CD4$^+$ T cells induces CTLA-4 blockade–associated colitis via Fcγ receptors

Bernard C. Lo[1], Ilona Kryczek[2,3], Jiali Yu[2,3], Linda Vatan[2,3], Roberta Caruso[1], Masanori Matsumoto[1], Yosuke Sato[4], Michael H. Shaw[4], Naohiro Inohara[1], Yuying Xie[5], Yu Leo Lei[6], Weiping Zou[1,2,3], Gabriel Núñez[1]*

Immune checkpoint inhibitors can stimulate antitumor immunity but can also induce toxicities termed immune-related adverse events (irAEs). Colitis is a common and severe irAE that can lead to treatment discontinuation. Mechanistic understanding of gut irAEs has been hampered because robust colitis is not observed in laboratory mice treated with checkpoint inhibitors. We report here that this limitation can be overcome by using mice harboring the microbiota of wild-caught mice, which develop overt colitis following treatment with anti-CTLA-4 antibodies. Intestinal inflammation is driven by unrestrained activation of IFNγ-producing CD4$^+$ T cells and depletion of peripherally induced regulatory T cells through Fcγ receptor signaling. Accordingly, anti-CTLA-4 nanobodies that lack an Fc domain can promote antitumor responses without triggering colitis. This work suggests a strategy for mitigating gut irAEs while preserving antitumor stimulating effects of CTLA-4 blockade.

Monoclonal antibodies targeting CTLA-4, PD-1, and PD-L1 are widely used to promote antitumor immune responses in a range of human cancers, but can also lead to inflammatory toxicities, collectively referred to as immune-related adverse events (irAEs) (*1*–*3*). Colitis is a common and severe irAE that can lead to treatment discontinuation, particularly in patients receiving a CTLA-4 inhibitor alone or in combination with PD-1 inhibitors; intestinal inflammation triggered by CTLA-4 blockade typically involves the colon and is characterized by the accumulation of CD4$^+$ T lymphocytes and neutrophils in the intestinal tissue (*3*–*5*). Analyses of colitis-associated lymphocytes of melanoma patients receiving CTLA-4 and PD-1 inhibitors have further implicated the pathogenic contributions of tissue-resident CD8$^+$ T cells with cytotoxic features (*6*). Our understanding of the immunological mechanisms of immune checkpoint blockade (ICB)–induced colitis has been impeded by the lack of robust animal models of colitis caused by immune checkpoint inhibitors. Laboratory mice are highly resistant to intestinal inflammation following treatment with antibodies targeting immune checkpoints (*7*, *8*). Therefore, current models of ICB-induced colitis require supplemental interventions to induce colitis such as exposure to dextran sulfate sodium (DSS) or the use of gene-targeted mice predisposed to intestinal inflammation (*8*–*11*). Concurrently, there has been increasing evidence that the gut microbiota composition may play a role in the susceptibility to colitis induced by ICB therapy, although microbial alpha diversity was similar in patients who developed ICB-induced colitis compared with patients undergoing ICB who did not develop colitis (*12*–*14*). However, the immunological mechanisms and the role of the microbiota underlying irAEs in the gut remain poorly understood.

We sought to establish a model of ICB-induced colitis using mice colonized with a referenced gut microbiota originally derived from wild-caught mice, referred to as wild mouse microbiome-reconstituted (WildR) mice (*15*). Laboratory mouse strains colonized with free-living microbiota exhibit immunological features that more closely resemble humans thus overcoming some of the limited utility of animal models of human diseases associated with the artificially hygienic status of conventionally raised specific pathogen-free (SPF) mice (*16*–*18*). Previously, WildR mice were shown to provide a more reliable model than SPF mice for anticipating the outcome of clinical trials of immune-modulating biologics (*18*). Therefore, we hypothesized that mice harboring the WildR microbiota would be a suitable system to examine host-microbiota interactions relevant to ICB therapy and irAEs.

Immune checkpoint blockade triggers colitis in mice colonized with wild microbiota

To investigate the role of the gut microbiota in ICB-induced intestinal inflammation, we first utilized C57BL/6 [wild-type (WT)] mouse lines with dissimilar gut microbiota composition from various commercial vendors raised under SPF conditions in addition to mice colonized with the WildR microbiota. In our initial experiments, we challenged mice with a[illegible] CTLA-4 and anti-PD-1 antibodies because [illegible] blockade was associated with a higher clinical risk of incurring gut irAEs compared with single ICB treatments (*3*, *4*). We also relied on fecal lipocalin-2 (LCN-2) measurements to track the kinetics and severity of intestinal inflammation after starting ICB treatment (*19*). Consistent with previous reports (*7*, *8*), we did not observe induction of fecal LCN-2 in SPF WT mice originating from Jackson Laboratories (JAX), Taconic Biosciences, or Charles River Laboratories after treatment with anti-CTLA-4 and anti-PD-1 antibodies (fig. S1). By contrast, fecal LCN-2 was highly induced in WT mice colonized with WildR microbiota after two injections of dual immune checkpoint inhibitors, and the intestinal inflammation was sustained for up to 21 days of the ICB treatment course (fig. S1).

To directly assess the impact of the microbiota on host susceptibility to ICB-associated colitis, we colonized germ-free C57BL/6 (WT) mice with SPF JAX microbiota or WildR microbiota. Germ-free (GF) WT mice colonized with SPF JAX microbiota did not develop colitis following ICB as indicated by fecal LCN-2 measurements and assessment of gut histology (Fig. 1, A and B). Although GF WT mice colonized with WildR microbiota treated with isotype antibodies did not develop colitis, GF WT mice colonized with WildR microbiota injected with anti-CTLA-4 and anti-PD-1 antibodies lead to clear and sustained induction of fecal LCN-2 (Fig. 1A). In addition, severe immunopathology was observed in the large intestinal tissue sections of these animals characterized by epithelial damage, marked infiltration of inflammatory cells in the lamina propria and submucosa, crypt abscesses, and apoptotic cells in the crypt epithelium that are prominent features of the disease in humans (Fig. 1B) (*5*). In patients, immune checkpoint inhibitors can cause irAEs in multiple organs (*3*). In the current model, dual ICB induced immune cell aggregates in the liver at a higher frequency in GF mice colonized with WildR microbiota compared with GF mice colonized with SPF JAX microbiota (fig. S2, A and B). Meanwhile, minimal or no evidence of inflammation was detected in the kidneys, heart, or lungs after treatment with ICB (fig. S2, A and B).

We evaluated the bacterial composition of the microbiota by performing 16s ribosomal RNA sequencing of fecal pellets collected from the GF mice colonized with SPF JAX microbiota or WildR microbiota during treatment with dual ICB or isotype controls. The alpha diversity of the bacterial communities of SPF JAX microbiota and WildR microbiota represented by Shannon indexes were similar and unaltered by treatment with dual ICB (fig. S3A). Moreover, a nonmetric multidimensional scaling plot of Bray and Curtis dissimilarity

[1]Department of Pathology and Rogel Cancer Center, University of Michigan, Ann Arbor, MI 48109, USA. [2]Department of Surgery, University of Michigan, Ann Arbor, MI 48109, USA. [3]Center of Excellence for Cancer Immunology and Immunotherapy, Rogel Cancer Center, University of Michigan, Ann Arbor, MI 48109, USA. [4]Takeda Pharmaceuticals International Co., Cambridge, MA 02139 USA. [5]Department of Computational Mathematics, Science and Engineering, Michigan State University, East Lansing, MI 48824, USA. [6]Department of Periodontics and Oral Medicine, Rogel Cancer Center, University of Michigan, Ann Arbor, MI 48104, USA.
*Corresponding author. Email: gabriel.nunez@umich.edu

indexes of individual mice indicates that the bacterial community structures of SPF JAX microbiota and WildR microbiota are dissimilar (fig. S3B). Alterations in the WildR microbiota were also observed in response to dual ICB coinciding with intestinal inflammation (fig. S3B). To compare bacterial taxa of the WildR microbiota and SPF JAX microbiota, we performed linear discriminant analysis effect size (LEfSe). We identified 132 OTUs at greater than 97% nucleotide sequence identity, which were differentially abundant in the WildR microbiota compared with SPF JAX microbiota (fig. S3C). These findings suggest that the bacterial communities of the SPF JAX microbiota and free-living WildR microbiota are similarly diverse yet highly divergent.

To determine the contributions of adaptive immunity in the present model of ICB-driven colitis, we colonized GF WT or GF *Rag1*$^{-/-}$ mice lacking lymphocytes with WildR microbiota and challenged them with dual ICB or isotype antibodies. As colitis was triggered in GF WT mice colonized with WildR microbiota by dual ICB, GF *Rag1*$^{-/-}$ mice colonized with WildR microbiota did not develop colitis after treatment with dual ICB or isotype control antibodies (Fig. 1, C and D). Collectively, these data indicate that induction of colitis in mice by ICB requires both the microbiota of free-living animals and an intact adaptive immune response.

CTLA-4 blockade elicits intestinal inflammation driven by CD4$^+$ T cells and IFNγ

We then compared the respective contributions of antibodies targeting CTLA-4 or PD-1 in the development of ICB-driven gut inflammation. WildR microbiota mice treated with dual ICB or anti-CTLA-4 antibodies alone were similarly susceptible to intestinal inflammation as evidenced by matching fecal LCN-2 induction and disease severity in intestinal tissues (fig. S4, A and B). By contrast, WildR microbiota mice that received anti-PD-1 antibodies alone did not develop intestinal inflammation (fig. S4, A and B). These data indicate that CTLA-4 blockade is the principal driver of colitis in this microbiota-dependent model, which is consistent with human studies (*3*, *4*). Furthermore, profiling of cecal immune cells by flow cytometry revealed the accumulation of IFNγ$^+$, IL-17$^+$, and double positive IFNγ$^+$ IL-17$^+$ CD4$^+$ T helper (T_H) cells 9 days after commencement of CTLA-4 blockade coinciding with high disease severity indicated previously by fecal LCN-2 levels (Fig. 2A). We also observed the induction of IFNγ$^+$ CD8$^+$ T cells after treatment with anti-CTLA-4 antibodies (fig. S5). Consistent with the skewed IFNγ response, we found robust Tbet but relatively mild RORγt expression by CD4$^+$ T cells in the intestinal tissue, further highlighting a biased T_H1 response during ICB-mediated inflammation (Fig. 2B and fig. S6). Moreover, anti-CTLA-4 antibody–induced colitis was associated with an increase in multiple myeloid cell subsets including neutrophils, monocytes, macrophages, and dendritic cells in the gut (fig. S7, A and B).

Intestinal regulatory T cells (T_{regs}) expressing Foxp3 are critical for immune homeostasis and can be categorized as thymic-derived T_{regs} (tT_{regs}) or peripherally induced T_{regs} (pT_{regs}) which are responsive to the gut microbiota (*20*, *21*). In GF mice, most gut Foxp3$^+$ T_{regs} display features suggestive of thymic origin whereas the colonization with intact microbiota or select bacterial species results in the induction of pT_{regs} including a subset expressing RORγt (*22*–*28*). In assessing Foxp3$^+$ T_{regs}

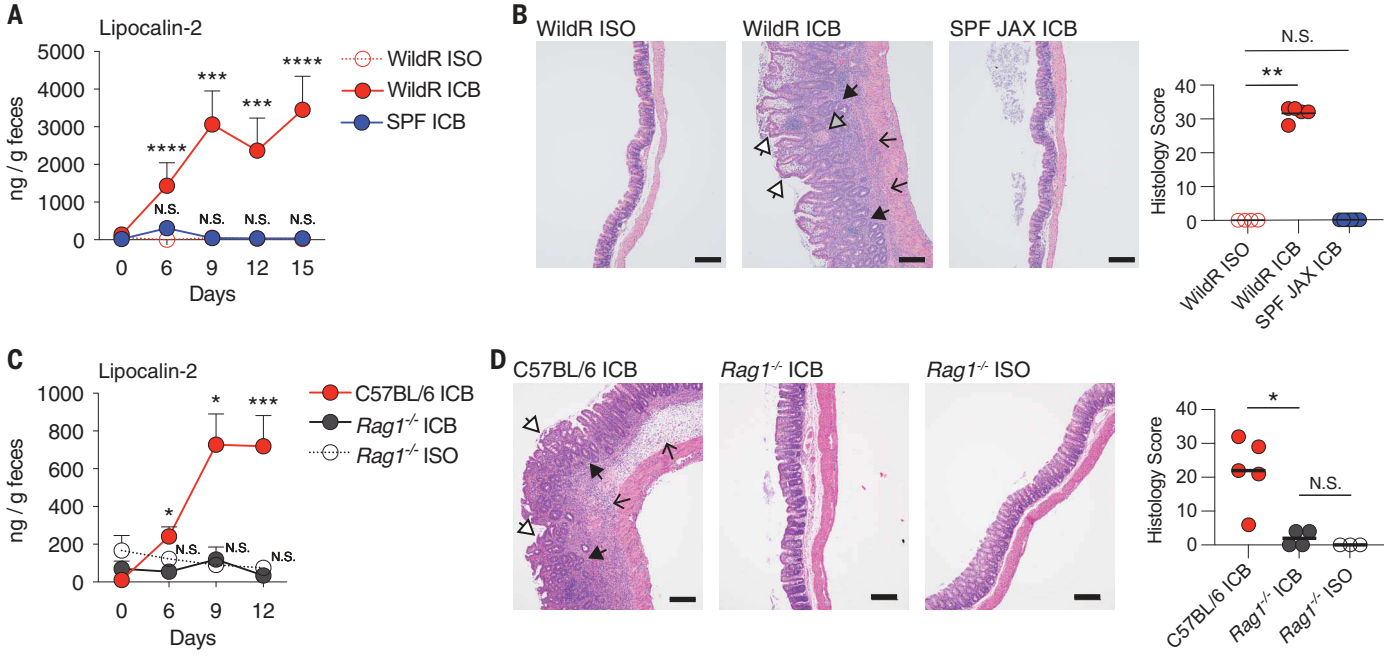

Fig. 1. Immune checkpoint blockade induces colitis in C57BL/6 mice harboring microbiota of wild-caught mice. (**A**) GF C57BL/6 (WT) mice were colonized with SPF JAX microbiota or WildR microbiota followed by treatment with anti-CTLA-4 antibodies and anti-PD-1 antibodies (ICB) or isotype (ISO) every 3 days. Colitis was assessed by fecal lipocalin-2. N.S., $P > 0.05$; ***, $P < 0.001$; ****, $P < 0.0001$ versus WildR ISO, Dunnett's multiple comparisons test. Data presented as mean ± SEM. (**B**) Hematoxylin and eosin (H&E)-stained sections of cecal tissues 15 days after starting ICB treatment, and histology scores. Scale bars, 200 μm. White arrowheads point to epithelial damage, black arrowheads point to regenerating epithelia, the gray arrow indicates a crypt abscess, and open arrows indicate inflammatory infiltrates. Each point represents an individual mouse. n = 4 to 6 mice per group. Representative data of two independent experiments. N.S., $P > 0.05$; **, $P < 0.01$, Kruskal-Wallis with Dunn's test. (**C**) GF C57BL/6 and GF *Rag1*$^{-/-}$ mice were colonized with WildR microbiota and treated with ICB or ISO. Colitis was assessed by fecal lipocalin-2. N.S., $P > 0.05$; *, $P < 0.05$; ***, $P < 0.001$ versus *Rag1*$^{-/-}$ ICB, Dunnett's multiple comparisons test. Data presented as mean ± SEM. (**D**) H&E-stained sections of cecal tissues 12 days after starting ICB treatment and histology scores. Scale bars, 200 μm. White arrowheads point to epithelial damage, black arrowheads point to regenerating epithelia, and open arrows indicate inflammatory infiltrates. Each point represents an individual mouse. n = 3 to 5 mice per group. Results were confirmed using SPF mice. N.S., $P > 0.05$; *, $P < 0.05$, Kruskal-Wallis with Dunn's test.

in the gut during ICB, we observed a reduction in the percentages of Foxp3$^+$ T cells (Fig. 2C) and notably the selective depletion of RORγt$^+$ pT$_{regs}$ whereas the relative percentages of a Helios$^+$ subset of tT$_{reg}$ cells remained largely intact (Fig. 2D). The reduction of RORγt$^+$ pT$_{regs}$ was confirmed in response to anti-CTLA-4 antibody treatment preceding peak inflammation (fig. S8, A and B). Previous reports demonstrate that RORγt$^+$ pT$_{regs}$ selectively induced by the microbiota possess distinct immunosuppressive features including exaggerated expression of CTLA-4, IL-10, and bacteria-reactive T cell receptors (TCRs) (*26*, *28*, *29*). Moreover, RORγt$^+$ pT$_{regs}$ are highly enriched in the large intestine but are mostly absent across systemic sites and in tumors (*28*). Consistent with previous studies, colonization of GF mice with WildR microbiota similarly induced RORγt$^+$ pT$_{regs}$ which have higher expression of CLTA-4 compared with a Helios$^+$ subset of tT$_{regs}$ (fig. S9, A and B). These data indicate that CTLA-4 blockade induces preferentially a T$_H$1 response and a biased depletion of RORγt$^+$ pT$_{regs}$ in the gut.

The accumulation of CD8$^+$ T cell subsets at mucosal surfaces is a common feature of laboratory mouse strains colonized with the microbiota of free-living animals (*16*, *18*). Moreover, tissue-resident CD8$^+$ T cell subsets with cytotoxic effector features have been implicated in the pathogenesis of ICB-induced colitis in the clinic (*6*, *30*), and we noted the induction of IFNγ$^+$ CD8$^+$ T cells in the present mouse model (fig. S5). To clarify the involvement of CD4$^+$ and CD8$^+$ T cells in ICB-driven intestinal inflammation, we selectively depleted each T cell subset in WildR microbiota mice during ICB treatment (fig. S10, A and B). Anti-CD8 antibodies delayed LCN-2 induction but had

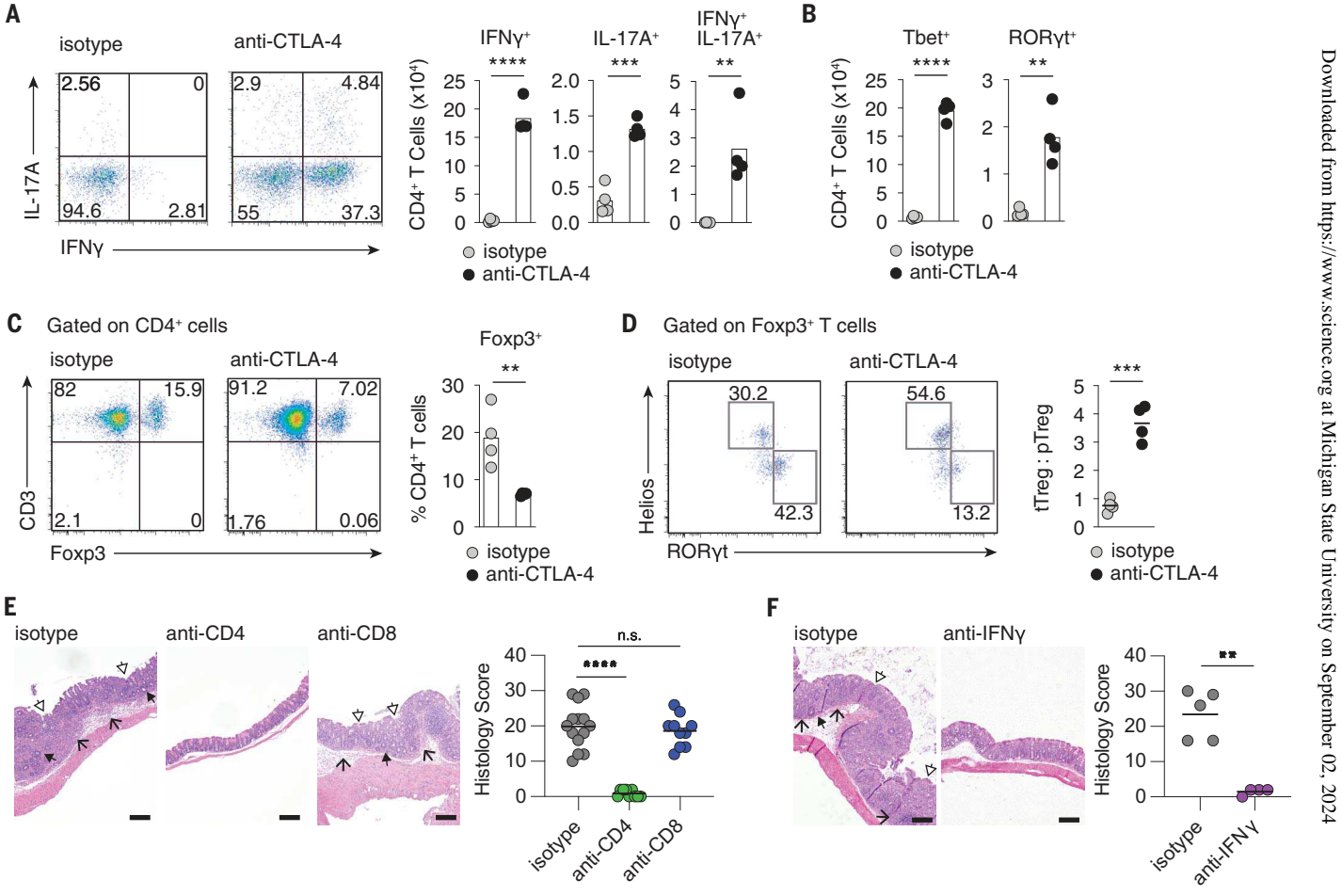

Fig. 2. Anti-CTLA-4 antibodies elicit IFNγ and CD4$^+$ T cell-mediated colitis. (**A**) FACS analysis of lymphocytes isolated from cecal tissues of WildR microbiota mice 9 days after starting anti-CTLA-4 antibody or isotype treatment. Pseudocolor plots depict IFNγ and IL-17 expression by CD4$^+$ T cells and numbers of cytokine-expressing CD4$^+$ T cells. Events displayed in flow plots: 2808, isotype and 6388, anti-CTLA-4 antibody-treated. (**B**) Numbers of Foxp3$^-$ CD4$^+$ T cells expressing Tbet and RORγt isolated from cecum. (**C**) Pseudocolor plots of Foxp3 expression by cecal T cells and percentage expression of Foxp3 by T cells. Events displayed in flow plots: 5906, isotype and 14803, anti-CTLA-4 antibody-treated. (**D**) Pseudocolor plot of Helios and RORγt expression by Foxp3$^+$ T cells and ratio of Helios$^+$ T$_{reg}$ (tT$_{reg}$) to RORγt$^+$ T$_{reg}$ (pT$_{reg}$) numbers. Events displayed in flow plots: 940, isotype and 1039, anti-CTLA-4 antibody-treated. Each dot represents an individual animal. n = 4 mice per group. Representative data of two independent experiments. **, $P < 0.01$; ***, $P < 0.001$; ****, $P < 0.0001$; unpaired two-tailed t-test. (**E**) WildR microbiota mice undergoing CTLA-4 blockade were treated with isotype control antibodies or cell-depleting antibodies against CD4 or CD8. H&E-stained cecal sections 12 days after starting ICB treatment and corresponding histology scores. Scale bars, 200 μm. White arrowheads point to epithelial damage, black arrowheads point to regenerating epithelia, and open arrows indicate inflammatory infiltrates. Each point represents an individual mouse. Data were combined from three independent experiments. N.S., $P > 0.05$; ****, $P < 0.0001$; Kruskal-Wallis with Dunn's test. (**F**) WildR microbiota mice receiving anti-CTLA-4 antibodies were treated with neutralizing anti-IFNγ antibodies or isotype control. H&E-stained cecal sections 12 days after starting ICB treatment, and histology scores. Scale bars, 200 μm. White arrowheads point to epithelial damage, the black arrowhead points to regenerating epithelium, and open arrows indicate inflammatory infiltrates. Each dot represents an individual mouse. Representative data of two independent experiments. **, $P < 0.01$; Mann-Whitney test.

no impact on reducing subsequent disease severity whereas mice that received antibodies that ablate CD4$^+$ cells were protected from ICB-induced gut inflammation (Fig. 2E and fig. S11). Furthermore, animals treated with IFNγ-neutralizing antibodies displayed highly diminished inflammation in the gut during the ICB treatment course (Fig. 2F). We also found that IL-17A/F KO mice displayed severity of gut immunopathology similar to that of WT mice in this disease model (fig. S12, A and B). Thus, intestinal inflammation triggered by CTLA-4 blockade in WildR mice is driven primarily by CD4$^+$ T cell–mediated responses and IFNγ.

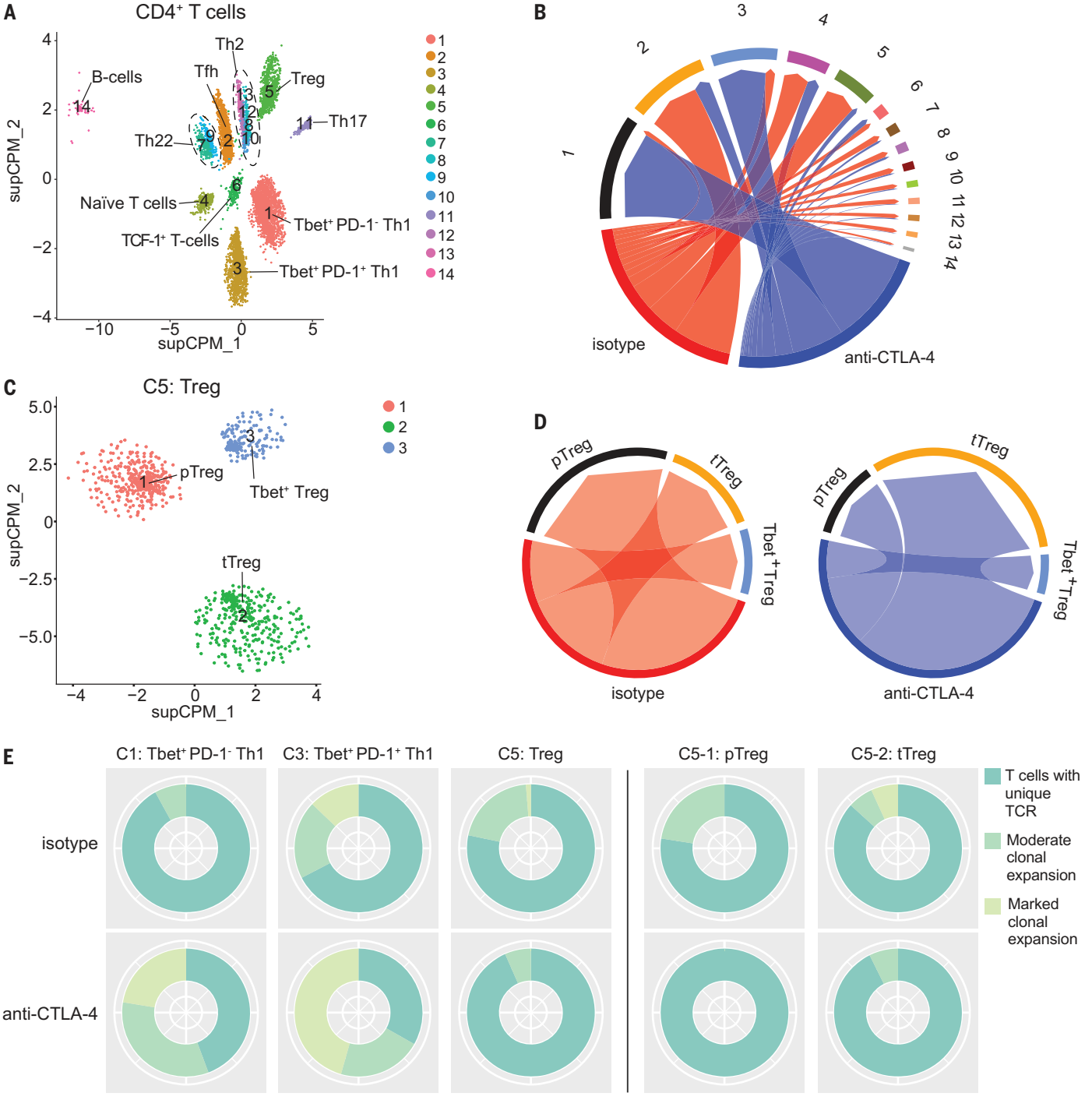

Fig. 3. Gene expression and clonotype analyses of CD4$^+$ T cells in ICB-induced colitis. (**A**) Sort-purified intestinal CD4$^+$ T cells from WildR mice treated with isotype or anti-CTLA-4 antibodies underwent scRNA-seq analyses; each sample contained pooled cells from tissues of 3 mice per treatment group. CD4$^+$ T cell clusters were visualized by supervised capacity preserving mapping (supCPM). (**B**) Circos plot showing relative contribution to each cluster identity by CD4$^+$ T cells from each treatment. (**C**) Cluster 5 T_{reg} cells were segregated and underwent further clustering and supCPM rendering and (**D**) circos plots showing relative abundance of each T_{reg} subcluster by treatment group. (**E**) Doughnut plots showing relative abundance of clonotypes in each cluster classified by three levels of clonal expansion. CD4$^+$ T cells with moderate clonal expansion include clonotypes with frequencies between two and four, and CD4$^+$ T cells with marked clonal expansion include clonotypes with frequencies of five or greater.

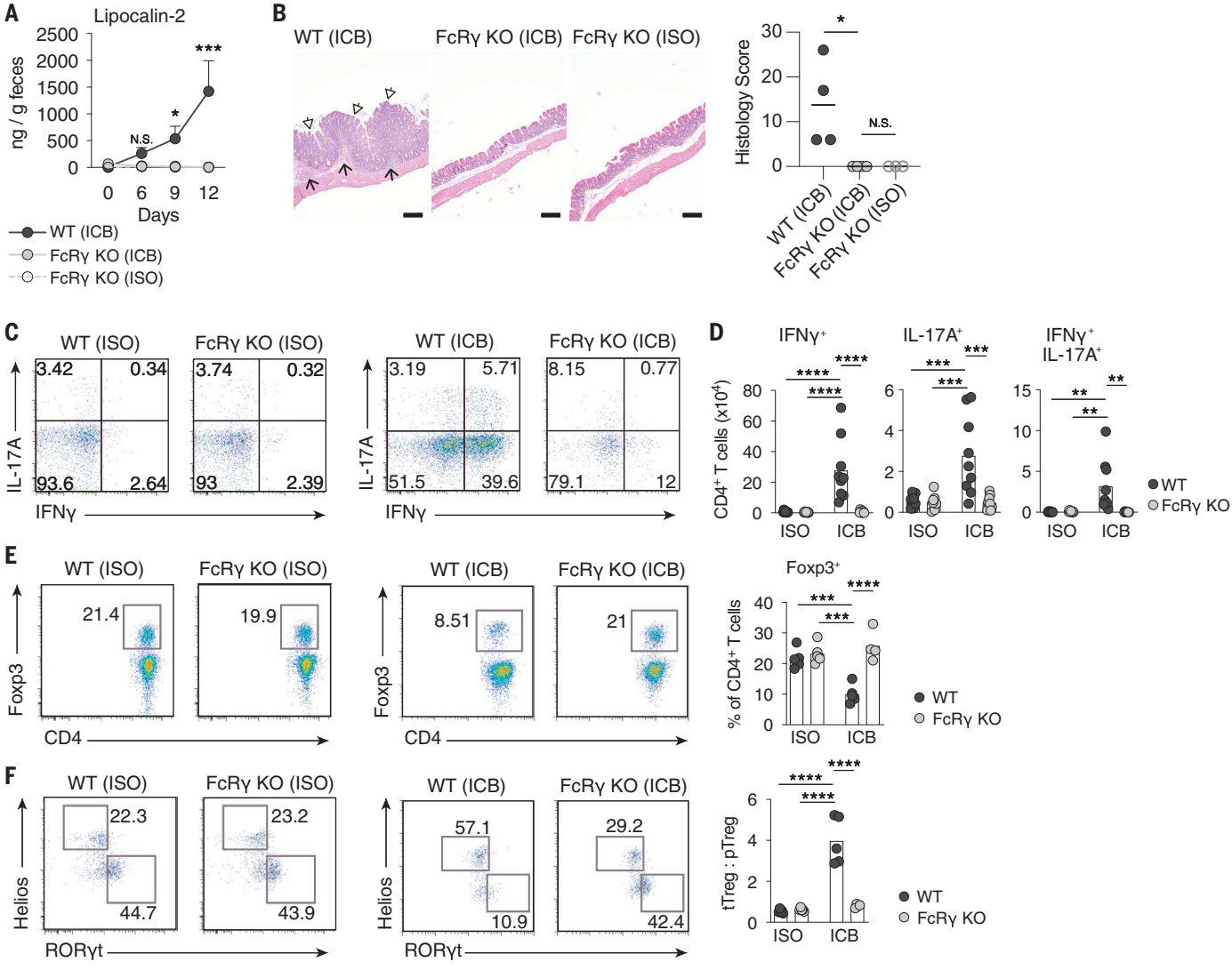

Fig. 4. Colitis induced by anti-CTLA-4 antibodies requires Fcγ receptors. (**A**) WT and *Fcer1g*$^{-/-}$ (FcRγ KO) mice were colonized with WildR microbiota and treated with anti-CTLA-4 antibodies (ICB) or isotype control antibodies (ISO). Colitis was assessed by fecal lipocalin-2. Statistical significance between ICB-treated WT and FcRγ KO mice was determined by Sidak's multiple comparisons test and indicated by N.S., $P > 0.05$; *, $P < 0.05$; ***, $P < 0.001$. Data presented as mean ± SEM. (**B**) H&E-stained sections of cecal tissues 12 days after starting indicated treatment and histology scores. Scale bars, 200 μm. White arrowheads point to epithelial damage and open arrows indicate inflammatory infiltrates. Each point represents an individual mouse. N.S., $P > 0.05$; *, $P < 0.05$; Kruskal-Wallis with Dunn's test. Representative data from two independent experiments. (**C**) Pseudocolor plots of cytokine expressing CD4$^+$ T cells isolated from ceca of WildR microbiota-colonized WT and FcRγ KO mice treated with isotype or anti-CTLA-4 antibodies. Events displayed in flow plots: 2949, WT (ISO); 2515, FcRγ KO (ISO); 8060, WT (ICB); 1165, FcRγ KO (ICB). (**D**) Numbers of cytokine-expressing T cells. Each point represents an individual mouse. Combined data from two independent experiments for each treatment group. **, $P < 0.01$; ***, $P < 0.001$; ****, $P < 0.0001$; Dunnett's multiple comparisons test. (**E**) Pseudocolor plots of Foxp3 expression by CD4$^+$ cells isolated from cecal tissues, and percentages of Foxp3 expression by T cells. Events displayed in flow plots: 5949, WT (ISO); 6487, FcRγ KO (ISO); 6664, WT (ICB); 4870, FcRγ KO (ICB). (**F**) Subsetting Helios$^+$ tT$_{regs}$ and RORγt$^+$ pT$_{regs}$, and the ratios of tT$_{regs}$ to pT$_{regs}$. Events displayed in flow plots: 1272, WT (ISO); 1293, FcRγ KO (ISO); 567, WT (ICB); 1024, FcRγ KO (ICB). Each point represents an individual mouse. Representative data from two independent experiments. ***, $P < 0.001$; ****, $P < 0.0001$; Dunnett's multiple comparisons test.

To assess whether ICB alters T$_{reg}$ subset abundance in a clinical setting, we examined a comprehensive single cell RNA sequencing (scRNA-seq) data set of intestinal immune cells isolated from ICB-treated melanoma patients who developed colitis, ICB-treated melanoma patients who did not develop colitis, and control cases (*6*). We utilized supervised capacity preserving mapping (supCPM) for cluster visualization (*31*) and observed diverse immune cell populations similar to clusters reported by the original investigators (fig. S13A and table S1) (*6*). We noted a singular T$_{reg}$ cluster (cluster 7), defined by high expression levels of *Foxp3*, *Ctla4*, *Il10*, and *Cd4*, which were elevated in relative abundance in ICB-treated patients who developed colitis compared with ICB-treated patients who did not develop colitis and normal control samples, which is consistent with the previous report (*6*) (fig. S13, A and B, and table S1). We further segregated the T$_{reg}$ cluster (cluster 7) and identified three T$_{reg}$ subclusters: T$_{reg}$ subcluster 7-1 was marked by high expression of Helios, encoded by *Ikzf2*; T$_{reg}$ subcluster 7-2 was defined by lower expression of *Ikzf2*; and T$_{reg}$ subcluster 7-3 was characterized by high expression of *Sell* and

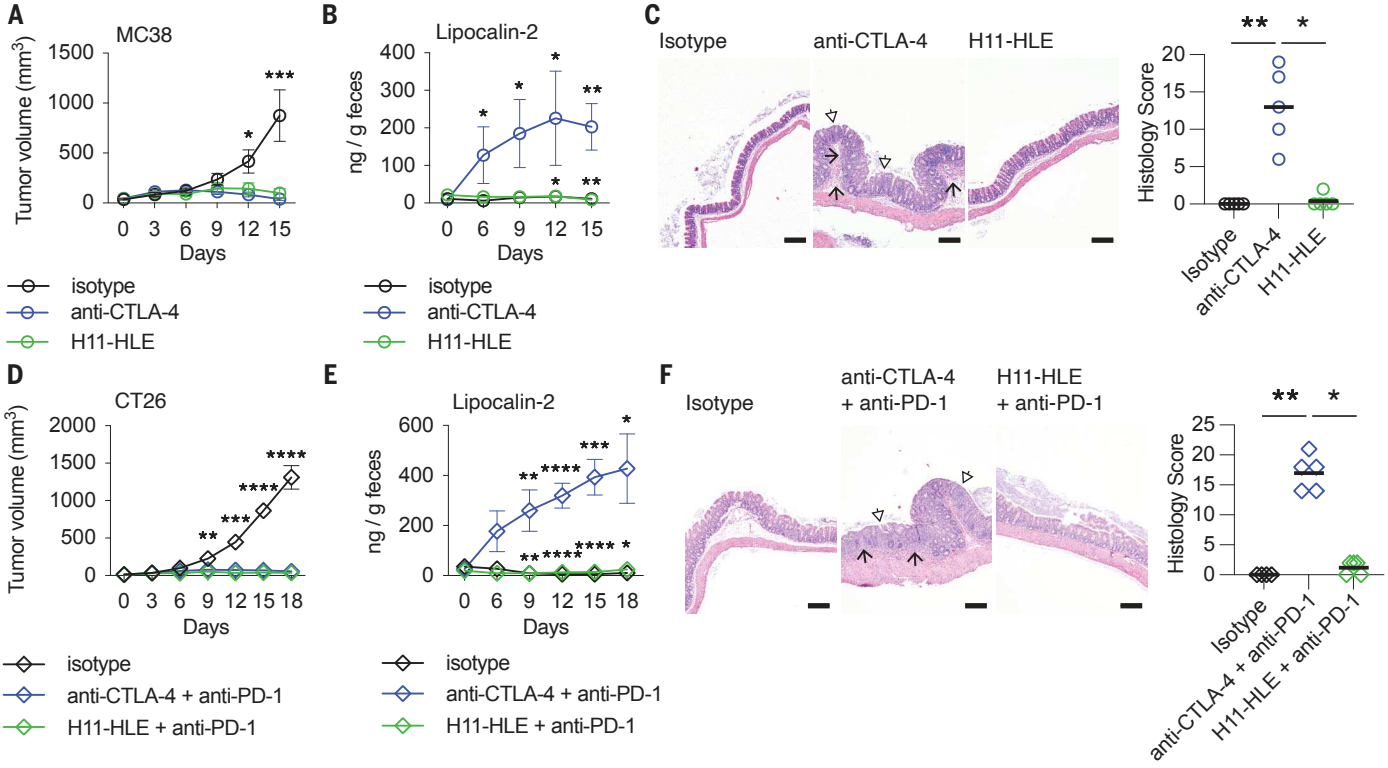

Fig. 5. Anti-CTLA-4 nanobodies stimulate anticancer immunity without inducing intestinal inflammation. (**A** to **C**) WildR microbiota-colonized WT mice were injected subcutaneously with MC38 tumor cells, then treated with isotype, anti-CTLA-4 antibodies, or anti-CTLA-4 H11 nanobodies with half-life extender (H11-HLE). Tumor volumes were tracked (A), and intestinal inflammation was assessed by fecal lipocalin-2 (B). (C) H&E-stained cecal sections 15 days after starting ICB treatment, and histology scores. Scale bars, 200 μm. White arrowheads point to epithelial damage and open arrows indicate inflammatory infiltrates. Each point represents an individual mouse. *, $P < 0.05$; **, $P < 0.01$; ***, $P < 0.001$; Dunnett's multiple comparisons test (A and B), or Kruskal-Wallis with Dunn's test (C) versus anti-CTLA-4 group. Top symbols denote *P*-values of comparison with isotype treatment group and bottom symbols denote *P*-values of comparison with H11-HLE treatment group (B). Data presented as mean ± SEM (A and B). Representative data of two independent experiments. (**D** to **F**) BALB/c mice colonized with WildR microbiota were injected subcutaneously with CT26 tumor cells, then treated with isotype, anti-CTLA-4 antibodies and anti-PD-1 antibodies, or H11-HLE and anti-PD-1 antibodies. Tumor volumes were tracked (D), and intestinal inflammation was assessed by fecal lipocalin-2 (E). (F) H&E-stained cecal sections 18 days after starting ICB treatment and histology scores. Scale bars, 200 μm. White arrowheads point to epithelial damage and open arrows indicate inflammatory infiltrates. Each point represents an individual mouse. *, $P < 0.05$; **, $P < 0.01$; ***, $P < 0.001$; ****, $P < 0.0001$; Dunnett's multiple comparisons test (D, E), or Kruskal-Wallis with Dunn's test (F) versus anti-CTLA-4 and anti-PD-1 group. Top symbols denote *P* values of comparisons with isotype treatment group, and bottom symbols denote *P*-values of comparisons with H11-HLE and anti-PD-1 treatment group (E). Data presented as mean ± SEM (D and E). Representative data of two independent experiments.

Ccr7 (fig. S13, C and D). Although human T_{reg} subset-defining transcripts remain imperfect, high *Ikzf2* expression may aid in the identification or enrichment of human tT_{regs} (*32*, *33*). We found that the *Ikzf2*^{hi} tT_{reg} subcluster 7-1, the most abundant T_{reg} subset, was similarly elevated in patients undergoing ICB therapy who developed colitis as well as ICB-treated patients who did not develop colitis compared with control cases (fig. S13E). By contrast, the relative proportion of the *Ikzf2*^{lo} nonthymic T_{reg} subcluster 7-2 was diminished in ICB-treated patients who had developed colitis compared with ICB-treated patients who did not develop colitis or control cases (fig. S13E). Moreover, the percentage of *Ikzf2*^{lo} T_{reg} subcluster 7-2 is sustained in ICB-treated patients who did not develop colitis compared with control cases (fig. S13E). T_{reg} subcluster 7-3 abundance was unaltered across patient groups. These data suggest that nonthymic T_{reg} persistence is selectively associated with intestinal homeostasis during ICB therapy.

CTLA-4 blockade induces oligoclonal T_H1 cells with cytotoxic features

Considering the pathogenic contributions of $CD4^+$ T cells in the current mouse model of CTLA-4 blockade–associated colitis, we sought to further define $CD4^+$ T cell responses by single cell transcriptomics. Sort-purified $CD4^+$ T cells from the intestinal tissues of isotype or anti-CTLA-4 antibody-treated mice were labeled with hashtag antibodies to minimize batch effects, and pooled samples underwent droplet-based scRNA-seq for gene expression and paired TCRα and TCRβ clonotype analyses. After filtering out cells with mitochondrial DNA content over 25% and those with a unique molecular identifier of <200 or >7500, we acquired 9671 high-quality transcriptomes. We clustered cells by using the top 5000 most differentially expressed genes and a panel of markers to stabilize immune lineage segregation (fig. S14 and table S2). To better preserve the accurate correlation between geographic distance and biological distance and improve the visualization of intracluster variance, we employed supCPM to project the clusters onto a two-dimensional space (*31*) (Fig. 3A). We identified nine $CD4^+$ T cell functional subsets and a small cluster of B cells (Fig. 3A and fig. S14). Following anti-CTLA-4 antibody treatment, we found a selective and marked increase in $IFN\gamma^+$ $Tbet^+$ T_H1 cells defined by clusters 1 and 3 which were mostly absent in isotype-treated mice (Fig. 3, A and B). One of the T_H1 clusters showed enhanced expression of PD-1 (cluster 3) and was further distinguished by elevated expression of transcripts related to cytotoxicity

(*Gzma*, *Gzmb*, *Prf1*) and chemokines (*Ccl3*, *Ccl4*, *Ccl5)* involved in myeloid cell responses (Fig. 3, A and B, and fig. S15A). Anti-CTLA-4 treatment resulted in a decrease in the relative abundance of follicular helper T-cells, naïve $CD4^+$ T cells, T_{regs}, $Tcf7^+$ $CD4^+$ T cells, T_H22 cells, T_H17 cells, and T_H2 cells (Fig. 3, A and B). To better assess the impact of anti-CTLA-4 treatment on distinct T_{reg} subsets, we separated cluster 5 and performed further clustering and supCPM rendering. We observed three distinct T_{reg} clusters: pT_{reg} (cluster 5-1), tT_{reg} (cluster 5-2), and an intermediate T_{reg} subcluster defined by elevated Tbet expression (cluster 5-3) (Fig. 3C and table S3). Consistent with previous findings, anti-CTLA-4 antibody treatment resulted in the selective depletion of pT_{regs} (42% reduction compared with isotype-treated mice) whereas tT_{regs} and $Tbet^+$ T_{regs} remained intact (Fig. 3D). Although most cells from T_H1 clusters 1 and 3 of the isotype-treated mice expressed unique TCRs, CTLA-4 blockade led to a substantial increase in the frequency of clonally expanded T_H1 cells whereas a major portion of clonally expanded T_{regs} were eliminated (Fig. 3E). Further assessment of clonotype abundance in T_H1 clusters 1 and 3 revealed that only five clonotypes with a frequency of 14 or higher were detected, all of which were selectively expanded by anti-CTLA-4 antibody treatment (fig. S15B). Among the five enriched clonotypes, a highly dominant clonotype (33% of C3 cells from anti-CTLA-4–treated mice) was observed in the cytotoxic $PD\text{-}1^+$ T_H1 cluster and was 14 times more abundant than the next most frequent clonotype within the same cluster (fig. S15B). Collectively, these observations indicate that colitic T_H1 cells are normally restricted under homeostatic conditions but can be selectively induced by anti-CTLA-4 antibodies in the presence of microbes of the WildR microbiota.

Colitis induced by anti-CTLA-4 antibodies requires depletion of T_{regs} by Fcγ receptors

The depletion of intratumoral T_{regs} by anti-CTLA-4 antibodies following Fcγ receptor (FcγR) engagement is thought to be one of the mechanisms involved in ICB-induced tumor rejection, although antitumor effects without T_{reg} depletion in tumor tissue have been observed in several studies (*34*–*40*). To test whether analogous Fc-dependent processes occur in the gut, we employed mice that lack the common FcRγ chain which is required for the assembly and function of FcγR family members (*41*). FcRγ-deficient mice colonized with WildR microbiota were highly resistant to intestinal inflammation following treatment with anti-CTLA-4 antibodies as demonstrated by minimal fecal LCN-2 induction during the course of ICB treatment and no evidence of immunopathology in cecal tissues compared with anti-CTLA-4 treated WT mice and isotype-treated FcRγ-deficient mice (Fig. 4, A and B). While we observed an increase in $CD4^+$ T cells expressing IFNγ, IL-17A, and both IFNγ and IL-17A in WT mice treated with anti-CTLA-4 antibodies, the induction of cytokine-producing $CD4^+$ T cells was not observed in FcRγ-deficient mice similarly receiving the anti-CTLA-4 antibodies nor mice receiving isotype antibodies (Fig. 4, C and D). Moreover, under anti-CTLA-4 antibody treatment conditions, the percentages of intestinal $Foxp3^+$ T_{regs} in WT mice were reduced compared with FcRγ-deficient mice and isotype-treated mice with a notable reduction in the proportion of $ROR\gamma t^+$ pT_{reg} (Fig. 4, E and F). These data suggest that FcRγ-dependent depletion of T_{regs} is required for gut inflammation in response to treatment with anti-CTLA-4 antibodies.

We further assessed the function of the anti-CTLA-4 antibody Fc domain during ICB-driven intestinal inflammation using a humanized mouse model of CTLA-4 blockade. We challenged a CTLA-4 transgenic mouse strain in which the extracellular and transmembrane domains of the mouse *Ctla4* sequence were replaced by the human ortholog (huCTLA-4 KI) with anti-human CTLA-4 antibodies containing a mouse IgG2a Fc domain (ipilimumab mIgG2a), or anti-human CTLA-4 antibodies with three amino acid substitutions (L234A, L235A, P329G) in the Fc domain (ipilimumab LALAPG) rendering the Fc domain inert to interact with FcγRs (*36*). We found that huCTLA-4 KI mice colonized with WildR microbiota and treated with ipilimumab mIgG2a developed intestinal inflammation as indicated by fecal LCN-2 levels and assessment of intestinal tissue sections (fig. S16, A and B). However, there was minimal or no indication of disease in huCTLA-4 KI mice colonized with WildR microbiota treated with ipilimumab LALAPG, and in huCTLA-4 KI mice re-colonized with SPF microbiota treated with ipilimumab mIgG2a (fig. S16, A and B). Results from this humanized CTLA-4 mouse model further highlight the requirement of a functional Fc domain for microbiota-dependent intestinal inflammation induced by ipilimumab.

Anti-CTLA-4 nanobodies stimulate antitumor immunity without inducing colitis

Given the requirement of Fc-FcγR interactions in the induction of colitis by anti-CTLA-4 antibodies, we hypothesized that camelid heavy chain–only antibody fragments (VHHs) or nanobodies which lack an Fc domain may be used for CTLA-4 blockade therapy while reducing the risk of gut irAEs. We utilized the CTLA-4-binding H11 VHH stabilized with a half-life extender (H11-HLE) that was previously found to exhibit anticancer activity in some settings (*35*, *36*). We sought to compare the antitumor activity of H11-HLE and anti-CTLA-4 antibodies in syngeneic tumor models; mice inoculated with tumors were also colonized with WildR microbiota to permit simultaneous tracking of ICB-mediated tumor rejection and colitis. First, to examine anticancer responses in a monotherapeutic checkpoint blockade setting, we inoculated mice subcutaneously with MC38 adenocarcinoma cells, and targeted CTLA-4. Compared with isotype-treated mice in which tumors grew as expected and reached the experimental endpoint by day 15 of the treatment course, we found that mice receiving anti-CTLA-4 antibodies displayed reduced tumor sizes by days 12 and 15 after starting CTLA-4 blockade (Fig. 5A and fig. S17, A and B). Furthermore, the same animals receiving anti-CTLA-4 blockade developed colitis as indicated by fecal LCN-2 induction during the treatment course and high histological disease scores in intestinal tissues compared with animals treated with isotype antibodies (Fig. 5, B and C). Notably, tumor-inoculated mice receiving H11-HLE exhibited similar antitumor activity as mice receiving antibodies against CTLA-4 but by contrast did not show evidence of colitis (Fig. 5, A to C, and fig. S17, A and B). While assessing MC38 intratumoral T cells—in comparison to the isotype control—the percentages of $Foxp3^+$ T_{regs} in $CD4^+$ T cells were reduced in animals treated with either anti-CTLA-4 antibodies or H11-HLE, though to a lesser extent (fig. S18, A to C). Moreover, treatment with anti-CTLA-4 antibodies did not alter the percentages of $Helios^+$ or $ROR\gamma t^+$ intratumoral T_{regs} compared with isotype controls thus indicating the tissue-specific effects of anti-CTLA-4 antibodies on large intestinal T_{reg} subsets (fig. S18, D to F). In addition, the frequencies of $CD4^+$ $Foxp3^-$ T cells among T cells were similarly elevated in tumors of mice treated with anti-CTLA-4 antibodies and H11-HLE compared with isotype controls (fig. S18G). Collectively, these data suggest that Fc domain–lacking nanobodies that block CTLA-4 can stimulate antitumor responses without inducing gut irAEs.

Combination CTLA-4 and PD-1 blockade can stimulate highly potent antitumor immune responses but also increase the risk and severity of irAEs (*3*, *4*). We therefore hypothesized that the use of the Fc-lacking H11-HLE CTLA-4 inhibitor with PD-1 blockade can provide similar therapeutic benefits while overcoming the limitations of its associated gut toxicities. To test this, we inoculated WildR microbiota mice with CT26 tumor cells which require both CTLA-4 and PD-1 blockade for efficient tumor rejection (*42*). We found that as tumors grew in isotype-treated animals, mice treated with anti-CTLA-4 antibodies and anti-PD-1 antibodies had similarly efficient antitumor responses compared with mice treated with H11-HLE and anti-PD-1 antibodies, as evidenced

by reduction in tumor sizes during the treatment course compared with isotype-treated controls (Fig. 5D and fig. S17, C and D). Moreover, only mice receiving both anti-CTLA-4 and anti-PD-1 antibodies developed colitis whereas isotype control mice or mice receiving H11-HLE and anti-PD-1 antibodies did not display evidence of intestinal inflammation (Fig. 5, E and F). We further evaluated the effects of H11-HLE nanobodies and conventional anti-CTLA-4 antibodies, in combination with PD-L1 blockade, in a syngeneic B16F0 melanoma implantation model (*43*). Treatment with H11-HLE and anti-PD-L1 antibodies was similarly effective as anti-CTLA-4 antibodies and anti-PD-L1 antibodies in limiting subcutaneous B16F0 tumor growth but did not induce overt intestinal inflammation (fig. S19, A to E). These results indicate the potential benefits of an Fc-lacking CTLA-4 inhibitor in combination with PD-1 or PD-L1 blockade without incurring the complications of colitis.

Discussion

The establishment of a robust animal model of ICB-driven colitis would be beneficial for gaining mechanistic insights into irAEs observed in the clinic and for improving current antitumor ICB therapies with reduced toxicities. In this study, we demonstrate the critical role of the microbiota in colitis induced by ICB and reveal key contributions of $CD4^+$ T_H1 cells and IFNγ in the pathogenesis of disease which is consistent with previously reported features of the human disease (*4*, *6*) (fig. S20). Several strategies have been proposed for suppressing colitis without altering the beneficial antitumor effects of ICB including neutralization of TNF or IL-6 (*8*, *9*). Moreover, the modification of the gut microbiota by fecal microbiota transplantation can mitigate intestinal inflammation induced by ICB (*44*). Here, we report that CTLA-4 inhibitors that lack an Fc domain do not induce colitis in mice which are otherwise susceptible to colitis when receiving conventional anti-CTLA-4 antibodies. Importantly, anti-CTLA-4 VHHs can effectively stimulate antitumor responses in mice without causing gut irAEs, thus circumventing the necessity for the neutralization of various pro-inflammatory cytokines or other strategies to modify the microbiota to remedy intestinal inflammation. These results also indicate that many immunological redundancies exist in the gut to prevent inappropriate T cell activation by the gut microbiota and that although the microbiota-induced T_{regs} are present, CTLA-4 blockade by itself is not sufficient to induce colitis.

In several genetic models, direct perturbation of gut pT_{regs} renders mice more susceptible to intestinal immunopathologies (*26*, *28*, *29*, *45*). Furthermore, mice lacking a population of tolerogenic $ROR\gamma t^+$ antigen-presenting cells, which are required for the induction of bacteria-reactive pT_{regs}, appear to develop intestinal inflammation associated with exaggerated pro-inflammatory T cell responses (*46*–*48*). However, CTLA-4 can also restrain T cell activation independently of T_{regs} in autoimmunity and antitumor responses (*49*, *50*). Therefore, further studies are needed to understand the potential cumulative effects of T cell CTLA-4 blockade and anti-CTLA-4 antibody-mediated depletion of T_{regs} during colitis.

We find that a CTLA-4 inhibitor lacking an Fc domain had similar antitumor immunity-promoting effects as conventional anti-CTLA-4 antibodies in mice harboring WildR microbiota. However, some—but not all—reports indicate that anti-CTLA-4 antibodies containing an Fc domain with high binding affinity to Fc receptors and functional Fc receptor activity is required for optimal tumor clearance through the selective depletion of intratumoral T_{regs} (*34*–*40*). This discrepancy may be explained, at least in part, by the dissimilarities in gut microbiota composition described in these animal models, as select gut bacterial strains or microbial communities have a profound impact on extra-intestinal immunity and responsiveness to CTLA-4 blockade for anticancer therapy (*51*–*53*). Given that the gut microbiota of free-living mice is highly immunogenic, the threshold of immune tolerance disruption required for activating optimal antitumor responses may be lower in WildR mice. Moreover, as recent data indicate that experimental mouse models that use the microbiota of free-living animals more accurately recapitulate human responses to immune-modulating therapies (*18*), our work provides evidence for the potential utility of an Fc-null anti-CTLA-4 antibody, either alone or in combination with PD-1 or PD-L1 blockade, in effectively stimulating anticancer immune responses without inducing intestinal inflammation.

REFERENCES AND NOTES

1. A. D. Waldman, J. M. Fritz, M. J. Lenardo, *Nat. Rev. Immunol.* **20**, 651–668 (2020).
2. W. Zou, J. D. Wolchok, L. Chen, *Sci. Transl. Med.* **8**, 328rv4 (2016).
3. F. Martins *et al.*, *Nat. Rev. Clin. Oncol.* **16**, 563–580 (2019).
4. E. Soularue *et al.*, *Gut* **67**, 2056–2067 (2018).
5. Y. Wang *et al.*, *Inflamm. Bowel Dis.* **24**, 1695–1705 (2018).
6. A. M. Luoma *et al.*, *Cell* **182**, 655–671.e22 (2020).
7. A. V. Heul, T. Stappenbeck, *J. Allergy Clin. Immunol.* **141**, AB119 (2018).
8. Y. Zhou *et al.*, *J. Exp. Med.* **220**, e20221333 (2023).
9. E. Perez-Ruiz *et al.*, *Nature* **569**, 428–432 (2019).
10. F. Wang, Q. Yin, L. Chen, M. M. Davis, *Proc. Natl. Acad. Sci. U.S.A.* **115**, 157–161 (2018).
11. K. Adam, A. Iuga, A. S. Tocheva, A. Mor, *PLOS ONE* **16**, e0246168 (2021).
12. M. C. Andrews *et al.*, *Nat. Med.* **27**, 1432–1441 (2021).
13. K. Dubin *et al.*, *Nat. Commun.* **7**, 10391 (2016).
14. R. C. Simpson *et al.*, *Nat. Med.* **28**, 2344–2352 (2022).
15. S. P. Rosshart *et al.*, *Cell* **171**, 1015–1028.e13 (2017).
16. L. K. Beura *et al.*, *Nature* **532**, 512–516 (2016).
17. D. Masopust, C. P. Sivula, S. C. Jameson, *J. Immunol.* **199**, 383–388 (2017).
18. S. P. Rosshart *et al.*, *Science* **365**, 6452 (2019).
19. B. Chassaing *et al.*, *PLOS ONE* **7**, e44328 (2012).
20. E. V. Russler-Germain, S. Rengarajan, C. S. Hsieh, *Mucosal Immunol.* **10**, 1375–1386 (2017).
21. T. Tanoue, K. Atarashi, K. Honda, *Nat. Rev. Immunol.* **16**, 295–309 (2016).
22. K. Atarashi *et al.*, *Science* **331**, 337–341 (2011).
23. G. J. Britton *et al.*, *Immunity* **50**, 212–224.e4 (2019).
24. M. B. Geuking *et al.*, *Immunity* **34**, 794–806 (2011).
25. S. K. Lathrop *et al.*, *Nature* **478**, 250–254 (2011).
26. C. Ohnmacht *et al.*, *Science* **349**, 989–993 (2015).
27. J. L. Round, S. K. Mazmanian, *Proc. Natl. Acad. Sci. U.S.A.* **107**, 12204–12209 (2010).
28. E. Sefik *et al.*, *Science* **349**, 993–997 (2015).
29. M. Xu *et al.*, *Nature* **554**, 373–377 (2018).
30. S. C. Sasson *et al.*, *Gastroenterology* **161**, 1229–1244.e9 (2021).
31. Z. Zhai, Y. L. Lei, R. Wang, Y. Xie, *Bioinformatics* **38**, 2496–2503 (2022).
32. K. R. James *et al.*, *Nat. Immunol.* **21**, 343–353 (2020).
33. A. M. Thornton *et al.*, *J. Immunol.* **184**, 3433–3441 (2010).
34. F. Arce Vargas *et al.*, *Cancer Cell* **33**, 649–663.e4 (2018).
35. D. Bauché *et al.*, *J. Immunother. Cancer* **8**, e001584 (2020).
36. Y. Sato *et al.*, *Cancer Immunol. Immunother.* **71**, 2421–2431 (2022).
37. A. Sharma *et al.*, *Clin. Cancer Res.* **25**, 1233–1238 (2019).
38. Y. Bulliard *et al.*, *J. Exp. Med.* **210**, 1685–1693 (2013).
39. M. J. Selby *et al.*, *Cancer Immunol. Res.* **1**, 32–42 (2013).
40. T. R. Simpson *et al.*, *J. Exp. Med.* **210**, 1695–1710 (2013).
41. T. Takai, M. Li, D. Sylvestre, R. Clynes, J. V. Ravetch, *Cell* **76**, 519–529 (1994).
42. K. Kim *et al.*, *Proc. Natl. Acad. Sci. U.S.A.* **111**, 11774–11779 (2014).
43. W. Wang *et al.*, *Nature* **569**, 270–274 (2019).
44. Y. Wang *et al.*, *Nat. Med.* **24**, 1804–1808 (2018).
45. H. Xu *et al.*, *J. Exp. Med.* **218**, e20210777 (2021).
46. B. Akagbosu *et al.*, *Nature* **610**, 752–760 (2022).
47. R. Kedmi *et al.*, *Nature* **610**, 737–743 (2022).
48. M. Lyu *et al.*, *Nature* **610**, 744–751 (2022).
49. W. Ise *et al.*, *Nat. Immunol.* **11**, 129–135 (2010).
50. K. S. Peggs, S. A. Quezada, C. A. Chambers, A. J. Korman, J. P. Allison, *J. Exp. Med.* **206**, 1717–1725 (2009).
51. L. F. Mager *et al.*, *Science* **369**, 1481–1489 (2020).
52. T. Tanoue *et al.*, *Nature* **565**, 600–605 (2019).
53. M. Vétizou *et al.*, *Science* **350**, 1079–1084 (2015).

ACKNOWLEDGMENTS

The authors thank K. Martin and A. Aboud for animal husbandry, P. Kuffa for laboratory management, T. Duval, L. Keeton, and L. Kennedy of the University of Michigan (UM) Germ-Free Animal Core, T. Tamsen and M. Coon of the UM Advanced Genomics Core, W. Trim and A.M. Deslauriers of the UM Flow Cytometry Core, S. McClintock of the UM Pathology Flow Cytometry Core, C. Strayhorn of the UM Dentistry Histology Core, K. Warren of the UM Tissue and Molecular Pathology Histology Core, and the UM Host Microbiome Initiative. **Funding:** This work was supported by NIH grants R01 DK121504 and R01 DK095782 and a grant from Takeda/Millennium Pharmaceuticals (to G.N.). B.C.L. was supported by a Canadian Institutes of Health Research Fellowship. Additional funding provided by a Crohn's and Colitis Foundation Senior Research Award (to R.C.), NIH grants R01 DE026728 and R01 DE030691 (to Y.L.L.), and NSF grant IOS-2107215 (to Y.X.). Research reported in this publication was supported by the National Cancer Institutes of Health under Award Number P30 CA046592 by the use of the following Cancer Center Shared Resources: Single Cell Spatial Analysis, and Tissue and Molecular Pathology. **Author contributions:** B.C.L., I.K., J.Y., L.V., R.C., and M.M. performed experiments, and analyzed data. Y.S. and M.H.S. provided advice, discussion, and critical materials. N.I. performed 16s rRNA analysis, and Y.X. and Y.L.L. performed single-cell immune profiling analyses. W.Z. designed experiments and provided advice. B.C.L. and G.N. conceived the project and designed experiments. G.N. supervised the study. B.C.L and G.N. wrote the manuscript with input from all authors. **Competing interests:** Y.S. and M.H.S. are employees of Takeda Pharmaceuticals International Co., Cambridge, MA, U.S.A. The other authors declare that they have no competing interests. **Data and materials availability:** C57BL/6

mice harboring WildR microbiota were obtained from Taconic Biosciences via a material transfer agreement. Fecal microbiota 16s sequencing data and single $CD4^+$ T cell RNA sequencing data are available at the NCBI SRA under BioProject number PRJNA944829.

SUPPLEMENTARY MATERIALS

science.org/doi/10.1126/science.adh8342
Materials and Methods
Figs. S1 to S20
Tables S1 to S3
References (54–60)

Submitted 16 March 2023; resubmitted 8 September 2023
Accepted 17 November 2023
10.1126/science.adh8342